Light scattering into silicon-on-insulator waveguide modes by random and periodic gold nanodot arrays

S. H. Lim, D. Derkacs, and E. T. Yu[a)]
Department of Electrical and Computer Engineering, University of California, San Diego, La Jolla, California 92093-0407, USA

(Received 20 October 2008; accepted 16 February 2009; published online 1 April 2009)

Experimental characterization and finite-element numerical simulations of the electromagnetic interaction between random or periodic Au nanodot arrays patterned atop a silicon-on-insulator (SOI) photodetector and incident electromagnetic plane waves have been performed at wavelengths of 400–1100 nm. The presence of the Au nanodots is found to lead to increased electromagnetic field amplitude within the semiconductor and, consequently, increased photocurrent response for both cases. Random arrays tend to exhibit broad increases in photocurrent over wavelength, whereas periodic arrays demonstrate sharp resonance peaks in the photocurrent absorption spectrum. Such features are due to the coupling of normally incident light into waveguide modes that satisfy the Bragg diffraction condition. Analysis of the dispersion relation of the waveguide modes allows for accurate prediction of the resonance peaks in the photocurrent absorption spectrum of the SOI photodetectors patterned with periodic nanodot arrays. © *2009 American Institute of Physics*.
[DOI: 10.1063/1.3100214]

I. INTRODUCTION

The electromagnetic behavior of metallic nanoparticles in the optical wavelength regime is of interest for semiconductor optoelectronic devices because of the strong absorption and scattering properties of such particles arising from their surface plasmon polariton resonances.[1–3] A number of applications of metallic nanoparticles integrated with semiconductor optoelectronic devices have been explored in recent research. Gold nanoparticles deposited on top of Si semiconductor photodiodes have been exploited to achieve greater optical absorption in the semiconductor via nanoparticle scattering around the plasmon polariton resonant wavelength,[4] and similar behaviors with thin film solar cells[5] and SOI photodetectors have also been demonstrated.[6,7] In device structures supporting waveguide modes, particularly large enhancements in photocurrent response can be attained due to the effect of light trapping in the semiconductor thin film.[8] Similarly, two-dimensional periodic dot arrays atop a slab waveguide[9,10] have also been studied. In these studies, the extinction or transmission characteristics of the structures were shown to be controllable by carefully tuning the nanodot array.

In this paper, we combine the use of periodicity with the presence of waveguide modes to achieve absorption enhancement in a silicon-on-insulator (SOI) photodetector. The periodically patterned dots are found to lead to photoabsorption enhancement of a different nature as compared with randomly patterned dots. The wavelengths at which enhancement occurs can be predicted and engineered by standard eigenvalue calculations of the characteristic waveguide modes and satisfaction of momentum conservation for photon scattering processes in periodic structures. Physically the periodic dot array imparts an additional momentum unto the photons which allow them to couple to waveguide modes. We also study the case of randomly patterned dots to assess the nature and size of effects associated specifically with periodicity rather than from scattering characteristics of isolated nanodots.

II. EXPERIMENT

SOI photodetectors of the photoconducting type were employed in these experiments. SOI wafers (Soitec) with 205 nm Si layer thickness (p-type, dopant concentration $\sim 10^{15}$ cm^{-3}) and 400 nm buried oxide thickness were cleaned using standard solvents and patterned to form Si mesas, as shown in Fig. 1. The two mesas were formed side by side by reactive ion etching of the top Si layer after masking the mesa areas with photoresist. A 100 nm Al/100 nm Au layer was then deposited on top of the Si mesas to form Ohmic contacts as well as the interconnects to large contact pads for probing.

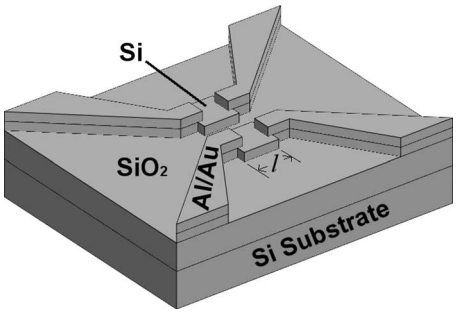

FIG. 1. Schematic diagram of the photoconductor device pair employed in the photocurrent response measurements. The thickness of the SiO_2 layer is 400 nm and the etched Si mesa layer is 205 nm with $l=180$ μm. One device has nanodots patterned on the surface between the contacts (not shown), while the other device has a smooth unpatterned surface.

[a)]Electronic mail: ety@ece.ucsd.edu.

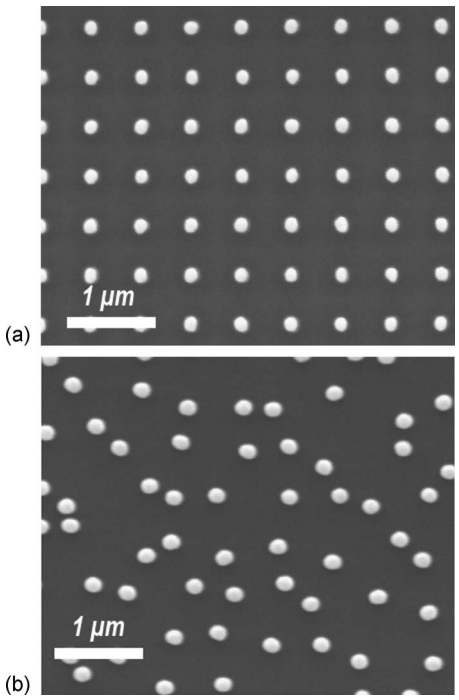

FIG. 2. Scanning electron micrographs of (a) periodic and (b) random Ti/Au nanodots patterned on SOI photoconductor surface by electron beam lithography.

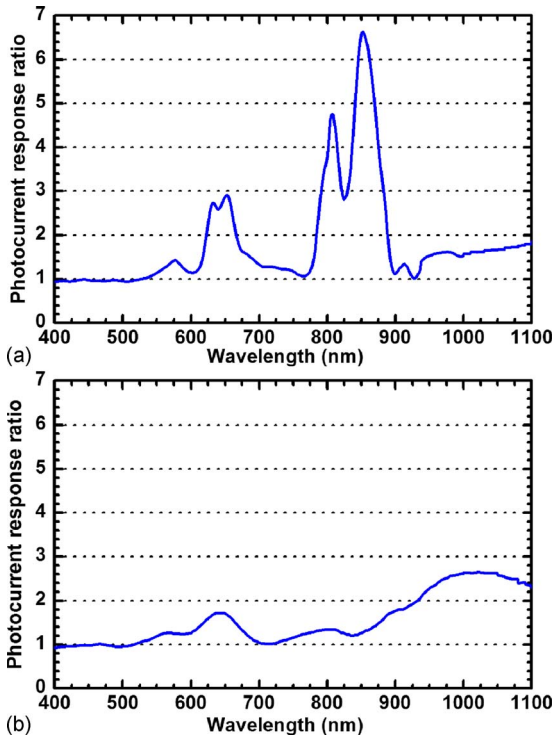

FIG. 3. (Color online) Measured photocurrent enhancement of SOI photoconducter due to (a) periodically patterned Ti/Au nanodots and (b) randomly patterned Ti/Au nanodots.

On one device of each pair, as shown in Fig. 1, 15 nm Ti/65 nm Au nanodot arrays are patterned over the exposed Si region by electron beam lithography, while the other device is left unpatterned as a reference. For the periodic nanodot structure, the nanodots are arranged in a square array with lattice spacing $a=550$ nm, while for the random nanodot array, the dot density is $\sim 3.31\times 10^8$ cm^{-2}, which is equal to the density of dots in the periodic array. In both cases, the dot diameter is ~150 nm. The shape of the nanodots turned out to be tapered rather than cylindrical. Scanning electron micrographs of devices with periodic and random nanodot arrays are shown in Fig. 2.

Spectral photocurrent response measurements were obtained for all devices using an apparatus that has been described in detail in a previous publication.[11] The devices were biased at 2.5 V through a dc biasing element. For each sample (having two devices side by side), a set of two measurements was obtained: the photocurrent response spectrum of the reference device as a function of wavelength, and the photocurrent response spectrum corresponding to the nanodot patterned device.

The devices, being in close proximity to each other, are illuminated with a light spot much larger than the device dimensions and, therefore, receive practically identical levels of light intensity. The photocurrent response of the device with the nanodot array is normalized so that it is equal to the photocurrent response of the reference device in the range of 400–450 nm. Electromagnetic simulations (discussed in Sec. III) show that the nanoparticles have little influence on the photoabsorption spectrum in this range of wavelengths (<7% variation). Therefore this corrects for a global variation in photoresponsitivity between the two devices arising from differences in contact resistance and other undetermined factors due to process variation. However, there is also a wavelength-dependent site-to-site variation on the order of 10% in the range of 400–700 nm and gradually increasing to about 30% at 950 nm. Each device is measured in an on/off cycle over several days to ensure that stable photocurrent spectra are obtained.

III. RESULTS AND DISCUSSION

Figures 3(a) and 3(b) show photocurrent response spectra for devices with periodic and random nanodot arrays, respectively, normalized in each case to the photocurrent response spectrum of the adjacent reference device as described above. As shown in Fig. 3(b), substantial enhancements in photocurrent response for the random nanodot array are observed at wavelengths of ~550–700 nm and also at wavelengths of ~850 nm and greater, although in the latter case variations in the (low) absolute level of photocurrent response at long wavelengths make detailed quantitative interpretation in this wavelength range less reliable. From Fig. 3(a) we see that for the periodic nanodot array, much larger photocurrent enhancements—up to nearly a factor of 6—are obtained, but over relatively narrow ranges of wavelength compared to those observed for the random nanodot array.

To facilitate interpretation of these results, we performed numerical analysis of the electromagnetic behavior of the random and periodic nanodots. We model the problem of light absorption enhancement due to periodic nanodots on SOI photodetector structures as an electromagnetic boundary value problem using the finite-element method. The goal is to calculate the increase in electromagnetic energy density within the semiconductor thin film due to the nanodots. The

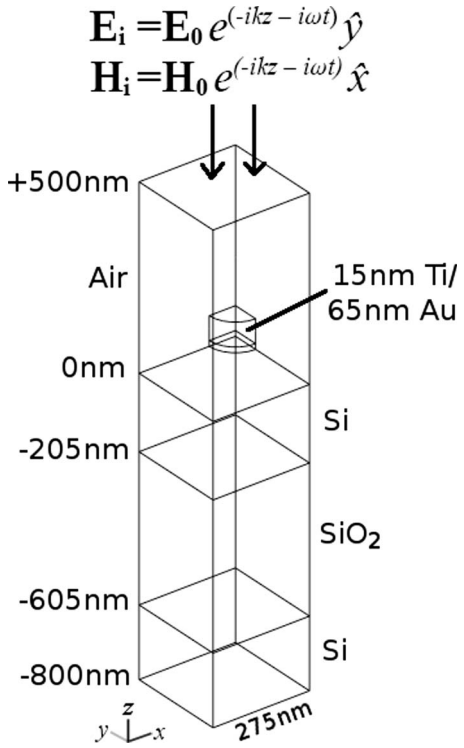

FIG. 4. One-quarter model geometry employed in the electromagnetic plane wave scattering simulation of a Ti/Au nanodot array on top of a SOI waveguiding layer, approximating the periodically patterned Ti/Au nanodot array on SOI experiment. A harmonic plane wave excitation, $\mathbf{E}_i(\mathbf{H}_i)$, is injected into the simulation volume through the top boundary.

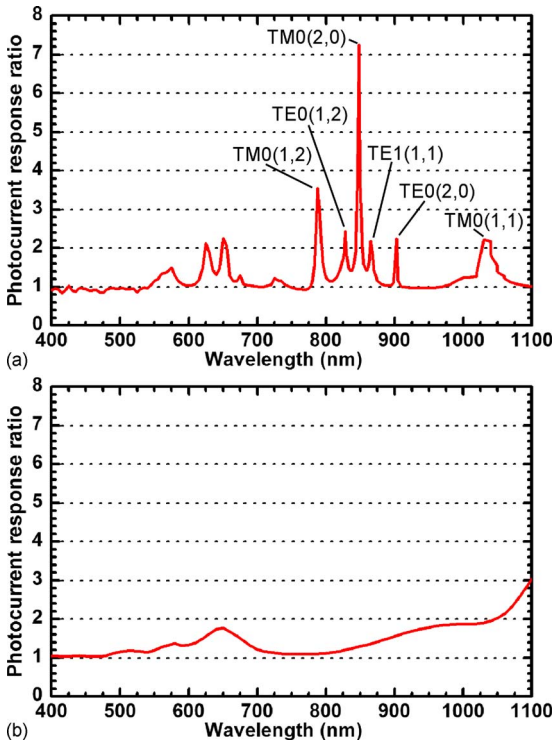

FIG. 5. (Color online) (a) Simulated electric field amplitude squared, $|\mathbf{E}|^2$, integrated over the Si thin film region of Fig. 4 normalized to $|\mathbf{E}|^2$ integrated over the same region in the absence of the Ti/Au nanodot array. The peak structures in the 750–1100 nm wavelength range are labeled according to the mode identification of Table I. (b) Calculated absorption enhancement due to randomly distributed dipole oscillators on SOI.

model geometry is shown schematically in Fig. 4, with the boundary conditions specified as in Ref. 11. In brief, the boundary conditions effectively impose periodicity to the solution,[12] so the solution actually corresponds to that for an infinite array of dots, which can be thought of as a metallic photonic crystal structure on a slab waveguide. Furthermore, only one-quarter of a unit cell needs to be simulated due to the constraints imposed by the cylindrical symmetry of the particle and the angle of the incident radiation, which is normal to the slab waveguide. For all numerical and analytical calculations, the wavelength-dependent dielectric functions of the optical materials employed were obtained from Ref. 13.

For the periodic nanodot array, the electromagnetic field distribution in this model is calculated at wavelengths ranging from 400 to 1100 nm and the square of the electromagnetic field amplitude, $|\mathbf{E}|^2$, is integrated in the top Si region as a proxy for optical absorption and photocurrent response. For the finite-element simulation, the model is discretized with a mesh of approximately 400 000 (400 K) elements. Mesh generation and assembly of the stiffness matrix and force vector were performed using the COMSOL™ Multiphysics RF module.[14] Obtaining the solution of the electromagnetic field then involves the factorization of a large sparse symmetric matrix roughly $450\,000 \times 450\,000$ in size. For this computation, we use the PARDISO solver[15,16] on a cluster supercomputer to parallelize the parametric sweep over wavelength.

Figure 5(a) shows a computation of $|\mathbf{E}|^2$ integrated over the silicon thin film within the simulation volume as a function of wavelength in the presence of the nanodot array, normalized to the integrated field intensity for the reference device structure without nanodots. Sharp peaks in photocurrent enhancement due to the periodic nanodot array are observed at wavelengths in generally good agreement with those for which photocurrent enhancement is observed experimentally. Certain aspects of the fine scale structure evident in the simulation results shown in Fig. 5(a) are not as apparent in the experimental results of Fig. 3(a), presumably due to fluctuations and minor imperfections in the experimentally realized structure that are not present in the simulation and to the finite experimental wavelength sampling resolution. Also, as previously noted, the experimentally fabricated nanodots are slightly tapered. This will affect the scattering cross section of the particles and, therefore, the absolute level of enhancement, but the location of the enhancement peaks should be unaffected.

For the analysis of the random nanodot array structure, we employ a method similar to previous calculations of absorption enhancement due to scattering by dipoles into silicon waveguides.[17] The nanodots are modeled as dipole oscillators, absorbing a portion of the incoming electromagnetic energy and re-emitting the energy into the waveguide and air. Incoming radiation is assumed to be separated into diffused and specular components.[18] The contribution of the specular component to the absorption can be calculated by the transfer matrix method. For the diffused component, light is assumed to undergo a repeated process of scattering off the rough surface (the interface patterned with

nanodots), reflecting off the smooth interfaces, and impinging once more on the rough surface. Therefore, the diffused component contribution is separated into an infinitely decaying series, with each term of increasing order denoting a later diffusion (scattering) step. This semiempirical model requires the determination of the diffused reflectance spectra $R(\lambda)$ of the nanodots on silicon. The experimental setup for determining such spectra is described by Leblanc *et al.*,[18] who also pointed out that $R(\lambda)$ can be calculated from the Mie theory. Due to the difficulty of measuring $R(\lambda)$ in our apparatus and the established validity of a computational approach, we have approximated the form of $R(\lambda)$ using the scattering cross section of spherical gold nanoparticles on silicon. The scattering cross section of gold nanoparticles in free space (Q_{sca}) can be calculated from the Mie theory. The presence of the silicon below the particle, however, modifies the scattering cross section[19] since the polarization of the nanoparticles will be modulated by the local driving field above the silicon substrate $\mathbf{E}_{loc}$.[20] This term can be very complicated to calculate, but the simplest approximation is given by the superposition of the incident plane wave and the reflected plane wave at the center of the nanoparticles, i.e., 40 nm above the substrate, yielding, $R(\lambda) \sim Q_{sca}|\mathbf{E}_{loc}|^2$. The result of this calculation for absorption enhancement is shown in Fig. 5(b), scaling $R(\lambda)$ to 0.0275 at $\lambda = 650$ nm. This parameter is chosen so that the absorption enhancement at 650 nm matches the experimentally measured absorption enhancement, and we can verify that the value chosen is physically very reasonable: The modified scattering cross section $Q_{sca}|\mathbf{E}_{loc}|^2$ is 0.489 at 650 nm, the fractional area coverage of the nanodots is 0.0584, and the proportion of incident flux converted into diffused flux can be approximated by the modified scattering cross section multiplied by the area coverage, which gives 0.0286. Finally, we note that the overall result of the model calculation is in good qualitative agreement with the experimental result of Fig. 3(b).

From the experimental and simulated results for photocurrent enhancement by periodically and randomly patterned nanodot arrays on SOI, we see that the presence of nanodots patterned atop a SOI device can lead to substantial enhancement in photosensitivity with a wavelength dependence that is strongly dependent on the spatial arrangement of the nanodots. The presence of nanodots causes normally incident light to scatter into waveguide modes,[6] effectively lengthening the optical path length of the photons in the Si thin film. Since the absorptance of the semiconductor decreases at longer wavelengths (700 nm and up), nanodot enhancement is more effective in this region.

Randomly distributed nanoparticles atop SOI have been shown to lead to enhancement of photocurrent response in a number of previous studies.[6,7] Our results for the randomly patterned dots are consistent with these previous results. Because we employed a relatively low density of dots ($\sim 3.31 \times 10^8$ cm^{-2}) in our experiments, we observe smaller enhancements compared to those reported previously. This is expected because scattering effects should generally increase with particle size and density. We also note that the enhancement for randomly distributed nanodots is mostly in the low absorptance region and is quite broad with limited wavelength selectivity.

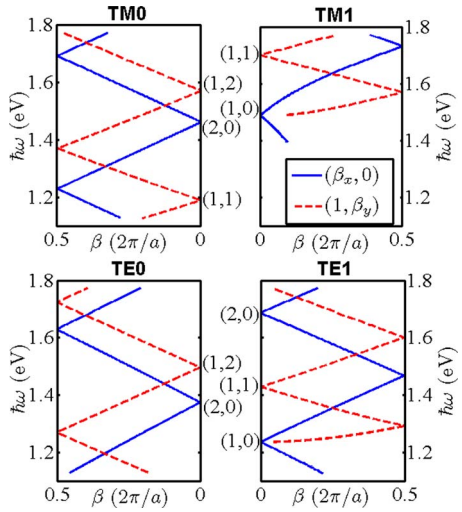

FIG. 6. (Color online) Dispersion curves (E vs β) where β is in units of $2\pi/a$ (a=550 nm) of the various TM and TE modes of the SOI structure plotted in a reduced zone scheme along the $(x,0)$ direction (solid) and $(2\pi/a, y)$ direction (dash) of the reciprocal lattice space. Each intersection of the dispersion curves with the ordinate axis corresponds to the Bragg condition $\beta = \sqrt{(nG)^2 + (mG)^2}$ with $G = 2\pi/a$ and is labeled by the vector (n,m).

In contrast, the enhancement due to periodically patterned dots is prominent only at certain wavelengths. As noted above, this is more clearly visible in the simulations than in the photocurrent measurements because fabrication related structural variations in the experimental nanodot array and the sampling resolution coarseness of the monochromator wash out some of the fine features of the photoabsorption spectral response. The location of each enhancement peak in Fig. 5(a) can be uniquely attributed to the presence of resonances in the extinction spectra of the nanodot array at certain wavelengths. Specifically, the location of each peak can be attributed to the resonant excitation of a waveguide mode by the normally incident photons. This is determined by the momentum conservation condition, $\beta = \sqrt{(nG)^2 + (mG)^2}$, where β is the waveguide mode's wavevector, $G = 2\pi/a$ is the reciprocal lattice constant of the periodic nanodot array, a=550 nm is the array periodicity, and n and m are integers. Physically, a normally incident photon cannot excite a waveguide mode because it has zero momentum in the plane of the waveguide. However, the periodic nanodot array imparts the additional momentum β unto the photons.

To determine the locations of the resonance peaks, we plot the dispersion relations of the SOI waveguide modes in a reduced zone scheme as shown in Fig. 6, with the dispersion curves folded back at the Brillouin zone edges π/a. The dispersion curves are plotted from ~700 to 1100 nm, or the cutoff frequency, whichever occurs first. Below 700 nm, the waveguide has too much absorption to support well defined modes, as will be evident later. Each intersection of the dispersion curve with the ordinate axis will represent a resonant frequency for Bragg diffraction of normally incident light

TABLE I. Table of the calculated energies and wavelengths at which the dispersion curves of the waveguide modes in the bare SOI structure intersects the ordinate axis of Fig. 6.

Mode(index)	Energy (eV)	λ (nm)
TM1(1,1)	1.7008	728.99
TE1(2,0)	1.6869	734.96
TM0(1,2)	1.5693	790.04
TE0(1,2)	1.4937	830.01
TM1(1,0)	1.4884	832.98
TM0(2,0)	1.4604	848.96
TE1(1,1)	1.4285	867.96
TE0(2,0)	1.3776	900.04
TE1(1,0)	1.2361	1003.1
TM0(1,1)	1.1894	1042.4

into waveguide modes of specific β and is therefore labeled by the diffraction order (n,m) involved in coupling the incident light into the waveguide mode. The values of the resonant frequencies and associated modes are shown in Table I. In reality, the presence of the nanodot array modifies the actual dispersion curves. However, since the particles are small and the scattering is weak, the frequency shifts due to dispersion modification can be neglected. This is similar to the case of corrugated waveguides with small groove depth.[21] Furthermore, a comparison of the predicted resonance frequencies with the numerical resonance peaks will confirm whether or not this assumption is valid.

Comparing the predicted resonant frequencies in Table I with the results shown in Fig. 5(a), we see that starting from 790 nm, each peak corresponds well with a particular mode. For example, the largest peak, appearing at 847.5 nm in the simulation, agrees well with the predicted location of the TM0(2,0) mode. Furthermore, a plot of the fields within the simulation volume, as shown in Fig. 7(a), at this wavelength clearly shows that there is a strong TM mode propagating along the Si thin film in the $\pm y$ direction with a period of 275 nm, half of the array period.

Because the TE0(1,2) and the TM1(1,0) modes are so close in wavelength, it is difficult to predict what will be the contribution of each mode to the observed peak at 828 nm. However, as can be seen in Fig. 7(b), the TE0(1,2) mode is the dominant mode. The modes at 730 and 735 nm do not show up as peaks in Fig. 5(a). This is expected as the absorption coefficient of the waveguiding Si layer increases rapidly below 800 nm. This means that any waveguide mode generated will have very short propagation lengths, and thus, exhibit weak resonance behavior. The mode at 1003 nm is very weak, whereas the mode at 1042 nm has a strong and broad peak. These effects are difficult to explain in the current theory and would perhaps require more detailed eigenfrequency calculations of the actual waveguide mode dispersion. Finally, comparing with Fig. 3(a), the modes at 900 nm and larger are not clearly detected in the photocurrent spectra. With further control of process variation and device instabilities, which tend to be particularly aberrant at the longer wavelengths, modes above 900 nm may be more apparent experimentally.

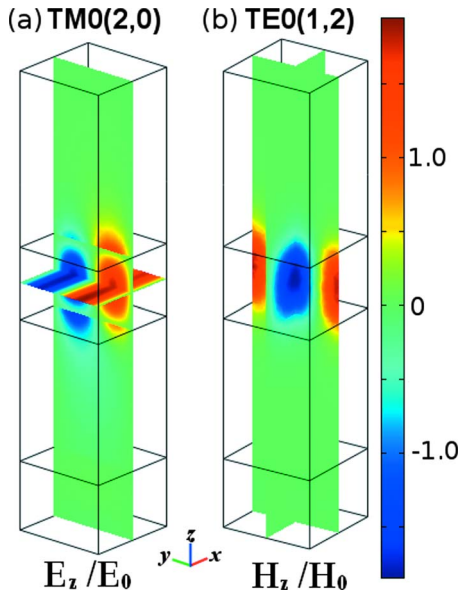

FIG. 7. (Color online) (a) Z component of the E field normalized to the incident plane wave amplitude $\mathbf{E}_0$ obtained from the electromagnetic scattering simulation of Ti/Au nanodot array on SOI at 847.5 nm showing the strong response of the TM0(2,0) mode to the incident plane wave excitation. (b) Z component of the normalized H field obtained at 828 nm. The field distribution clearly shows the strong response of the TE0(1,2) mode.

IV. CONCLUSION

We have studied the effect of nanodot array enhancement of optical absorption and photocurrent response for SOI photodetectors by experiment and numerical simulation. In particular, we examine and compare the cases of randomly and periodically patterned nanodot arrays to explicitly assess and analyze the consequences of dot periodicity. We see that the physical mechanism for photocurrent enhancement in SOI photodetectors is the same for the random and periodic nanodots, i.e., the scattering of plane waves into waveguide modes, which lengthens the photon propagation distance in the active layer. The major difference between the random and periodic nanodot arrays is the introduction of enhancement resonances in the case of the periodic array.

Enhancement from the randomly patterned dots is in agreement with previously reported results. On the other hand, enhancement from the periodically patterned dots is stronger for the same density of dots albeit confined to a narrower range of wavelengths. The simulation results are in generally good agreement with the experiments. In addition, simulations and theoretical analyses allow identification of photocurrent enhancement features observed experimentally with specific scattering and momentum conservation processes associated with the array periodicity. This study shows that it is possible to engineer wavelength specific enhancement on SOI photodetectors by considering and exploiting the effect of periodicity. This could also be beneficial for other types of optical conversion devices that are built from layered media, including a variety of photodetector structures and thin film photovoltaic devices.

ACKNOWLEDGMENTS

This research was supported in part by the National Science Foundation through TeraGrid resources provided by

SDSC and TACC and by AFOSR (Grant No. FA9550-07-1-0148). S.H.L. would like to acknowledge valuable discussions with P. R. Matheu concerning efficient solver methods for the simulations presented here.

[1]J. Kottmann, O. Martin, D. Smith, and S. Schultz, Opt. Express **6**, 213 (2000).
[2]K. L. Kelly, E. Coronado, L. L. Zhao, and G. C. Schatz, J. Phys. Chem. B **107**, 668 (2003).
[3]C. F. Bohren and D. R. Huffman, *Absorption and Scattering of Light by Small Particles* (Wiley, New York, 1983), pp. 93, 100-3, and 139.
[4]D. M. Schaadt, B. Feng, and E. T. Yu, Appl. Phys. Lett. **86**, 063106 (2005).
[5]D. Derkacs, S. H. Lim, P. Matheu, W. Mar, and E. T. Yu, Appl. Phys. Lett. **89**, 093103 (2006).
[6]S. Pillai, K. R. Catchpole, T. Trupke, and M. A. Green, J. Appl. Phys. **101**, 093105 (2007).
[7]H. R. Stuart and D. G. Hall, Appl. Phys. Lett. **69**, 2327 (1996).
[8]H. R. Stuart and D. G. Hall, Appl. Phys. Lett. **73**, 3815 (1998).
[9]G. Gantzounis, N. Stefanou, and N. Papanikolaou, Phys. Rev. B **77**, 035101 (2008).
[10]S. Linden, J. Kuhl, and H. Giessen, Phys. Rev. Lett. **86**, 4688 (2001).
[11]S. H. Lim, W. Mar, P. Matheu, D. Derkacs, and E. T. Yu, J. Appl. Phys. **101**, 104309 (2007).
[12]C. Hagglund, M. Zach, G. Petersson, and B. Kasemo, Appl. Phys. Lett. **92**, 053110 (2008).
[13]E. D. Palik, *Handbook of Optical Constants of Solids* (Academic, San Diego, 1985), pp. 290–295 and 555–568.
[14]L. Y. Tio, A. A. P. Gibson, B. M. Dillon, and L. E. Davis, Int. J. Electr. Eng. Educ. **41**, 1 (2004).
[15]O. Schenk and K. Gärtner, FGCS, Future Gener. Comput. Syst. **20**, 475 (2004).
[16]O. Schenk and K. Gärtner, Electron. Trans. Numer. Anal. **23**, 158 (2006).
[17]K. R. Catchpole and S. Pillai, J. Appl. Phys. **100**, 044504 (2006).
[18]F. Leblanc, J. Perrin, and J. Schmitt, J. Appl. Phys. **75**, 1074 (1994).
[19]P. A. Bobbert and J. Vlieger, Physica A **137**, 209 (1986).
[20]B. J. Soller and D. G. Hall, J. Opt. Soc. Am. B **19**, 1195 (2002).
[21]M. Nevière and E. Popov, *Light Propagation in Periodic Media: Differential Theory and Design* (Dekker, New York, 2003), pp. 309–313.